Synthetic Metals 280 (2021) 116881

Contents lists available at ScienceDirect

Synthetic Metals

journal homepage: www.elsevier.com/locate/synmet

Electrochemical formation of N–substituted polypyrrole nanowires, microwires and open microtubes and their decoration with copper structures

Conor P. McCarthy [a], Karen M. Herdman [a], Denise Rooney [a,b], Bernadette Alcock-Earley [a], Carmel B. Breslin [a,*]

[a] Department of Chemistry, Maynooth University, Maynooth, Co. Kildare, Ireland
[b] Kathleen Lonsdale Institute for Human Health Research, Ireland

ARTICLE INFO

Keywords:
N–substituted polypyrrole
N–(2–cyanoethyl)pyrrole
Nanowires
Microwires
Microtubes
Copper

ABSTRACT

The substituted pyrrole monomer, N–(2–cyanoethyl)pyrrole, was electropolymerised in a 70% water and 30% ethanol solution with ClO_4^- and $H_2PO_4^-$ as the dopant species to give nanowires at short electropolymerisation times and microwires at longer deposition periods. On adding toluene to the electropolymerisation solution, hollow microtubes were formed. This was attributed to the adsorption of toluene droplets at the electrode surface which served to separate the dopants from the monomer, with the monomer being highly soluble in the toluene droplet and the inorganic dopants soluble in the water/ethanol mixture. As a result electropolymerisation was confined to the toluene-water/ethanol interface. These polymer systems exhibit redox activity with the oxidation wave centred at about 0.40 V vs SCE, and the broader reduction wave positioned between 0.75 V and 0.25 V vs SCE. Although N-substitution reduces the conductivity of the polymer, various copper deposits, including cubes, leaves and hierarchical structures were deposited at the microwires and microtubes using high overpotentials. The hierarchical structures were wrapped around the microtubes at considerable distances, typically 3–4 μm, from the substrate.

1. Introduction

Conducting polymers, particularly polypyrrole, have attracted considerable interest in recent years as they are easily prepared using chemical polymerisation or electropolymerisation and readily combined with other materials, such as carbon nanotubes [1], graphene [2], graphitic carbon nitride [3] and various metal or metal oxide nanoparticles to give conducting hybrid materials with interesting properties [4,5]. They have a large number of applications, and have been utilised in the development of electrochromic devices [6], sensors [7,8], drug delivery systems [9,10], corrosion protection [11], batteries [12], capacitors and supercapacitors [13] and in microextraction [14].

More recently, there has been a focus on forming polypyrrole nanowires and nanostructures that possess more superior physical and chemical properties compared to their bulk counterparts [15,16]. Polypyrrole nanostructures are commonly formed using hard templates, such as anodic aluminium oxide [17,18] or zeolites [19], and soft templates, such as biological species [20,21] and adsorbed surfactant molecules [22], which can be employed as templates to control and orient the forming polymer. Synthesis using the soft template has the added advantage that the template does not require removal. Polypyrrole nanowires have also been generated using electropolymerisation by careful selection of the electropolymerisation solution and dopants [16,23,24]. This strategy is not only relatively simple, but it facilitates the deposition of the polypyrrole nanowires or nanostructures at a variety of different conducting substrates. The monomer is oxidised at the conducting substrate and by controlling the rate of electropolymerisation and the nature and concentration of the dopant anions in solution, nanowires can be fabricated. It has also been shown that the nanowires can be deposited at oxidisable substrates, such as Cu and Ni, using cathodic electropolymerisation in an aqueous nitrate solution, where electrochemically generated NO^+ facilitates the oxidation of the pyrrole monomer at the Cu or Ni cathode [25]. There is also considerable interest in using sulphonic azo dye molecules to direct the morphology of the growing polymer to give various polypyrrole nanostructures [26]. In this case, sulphonic azo dye aggregates are formed in

* Corresponding author.
E-mail address: Carmel.Breslin@mu.ie (C.B. Breslin).

https://doi.org/10.1016/j.synthmet.2021.116881
Received 8 June 2021; Received in revised form 26 July 2021; Accepted 7 August 2021
Available online 17 August 2021

acidic media and precipitate as one dimensional precipitates. These degrade gradually as the electropolymerisation reaction proceeds providing a hollow nanotube morphology [27,28].

Another way to alter the properties of the final polymeric structures is to form polypyrrole derivatives. Various N– and β–substituted polypyrrole films have been formed successfully [29–32] and these include polymers produced through the electropolymerisation of N-carboxyalkyl pyrrole [33], N–arylmethylene pyrrole [34], N–(2–cyanoethyl) pyrrole [35,36] and 3– and 3,4–methyl substituted pyrrole [37]. Most of these polymers are bulk substituted polypyrrole films, while there are relatively few reports to show that they can be formed as nanowires or as other tubular, nano- or micro-structures. McCarthy et al. [35,38] have electropolymerised N–(2–cyanoethyl)pyrrole to give open and closed microstructures, while Li et al. [39] employed a self-templating process to form β–FeOOH decorated hollow polymerised N–(2–cyanoethylpyrrole) microspheres using a self-templating approach.

In this paper, which is a continuation of our previous work to give open and closed N–substituted polypyrrole microstructures [35,38], we show that N–(2–cyanoethyl) pyrrole can be readily electropolymerised to give both nanowires, microwires and microtubes. By controlling the composition of the electropolymerisation solution and electropolymerisation conditions these structures can be formed in the absence of hard templates, Although this N–substituted polypyrrole has a lower conductivity that the corresponding unsubstituted polypyrrole, it is nevertheless possible to electrodeposit copper at these structures to give copper decorated PPyEtCN microwires and microtubes. While bulk polypyrrole has been used widely as a support for the electrochemical reduction of various metals and metal oxides, particularly copper oxides [40], there are no reports, to the best of our knowledge, to show that these less conducting substituted polypyrrole films can be decorated with copper electrodeposits. This copper metallisation has the potential to increase the applications of these substituted polypyrrole systems.

2. Experimental

All chemicals were of analytical grade and were obtained from Sigma-Aldrich, Dublin, Ireland. The monomers, pyrrole and N–(2–cyanoethyl) pyrrole (PyEtCN), were distilled under vacuum and stored at – 40 °C under an atmosphere of nitrogen. All other reagents were used as received. Prior to electropolymerisation, the PyEtCN was added to an ethanol-water (deionised) mixture, then the dopant salts were added with vigorous stirring. The larger open microstructures were formed using a similar solution but with the addition of toluene. Unless otherwise stated, the PPyEtCN nanowires and microwires were formed in a solution containing 0.075 M PyEtCN, 0.3 M $NH_4H_2PO_4$ and 0.02 M $LiClO_4$ dissolved in a 70% water, 30% ethanol solution at a fixed potential of 0.85 V vs SCE. The nanowires were formed using electropolymerisation periods less than 240 s, while the microwires were fabricated using longer electropolymerisation times. For comparison purposes, polypyrrole nanowires were formed from an aqueous solution containing 0.15 M pyrrole, 0.2 M Na_2HPO_4 and 0.02 M $LiClO_4$ at 0.80 V vs SCE for 300 s. Finally, the open microtubes were generated from the 70% water and 30% ethanol solution with 0.02 M $LiClO_4$, 0.3 M $NH_4H_2PO_4$, 0.075 M PyEtCN and 80 μL toluene dissolved in 10 mL of electropolymerisation solution. This suspension was stirred vigorously and then sonicated in an ultrasonic bath (Fisher Scientific FB 15048) for 1 min. Copper electrodeposition reactions were carried out in 0.05 M $CuSO_4$ with 0.050 M H_2SO_4 or 0.05 M Na_2SO_4 (adjusted to a pH of 4.0 using H_2SO_4) as the supporting electrolyte.

All electrochemical experiments were performed with a Solartron 1285 potentiostat using a three electrode cell, comprising a glassy carbon electrode (3 mm), a platinum mesh as a counter electrode and a saturated calomel reference electrode (SCE). As the ethanol content was maintained at 30% in the aqueous solution with phosphate and perchlorate ions, the SCE served as an appropriate reference electrode. The glassy carbon electrode was polished to a mirror finish using Buehler MetaDi monocrystalline diamond suspensions, 30–1 μm on a Buehler polishing microcloth. The electrodes were sonicated in ethanol and water for 300 s between each polishing step with a final 300 s sonication period. FTIR spectra were recorded using a Perkin Elmer 2000 FTIR spectrometer, while RAMAN spectra were obtained using a LABRAM high resolution Raman spectrometer. A Hitachi S-3200-N with a tungsten filament or a Hitachi S-4000 with a cold cathode field emission source (FE-SEM) were used to study the morphologies of the PPyEtCN structures and copper modified polymers. Energy dispersive X-ray (EDX) analyses was carried out using an Oxford Instrument INCAx-act EDX system.

3. Results and discussion

3.1. Water-ethanol solvent system and formation of bulk polymer

As the PyEtCN monomer has limited solubility in aqueous solutions, an ethanol-water system was selected to enhance the solubility of the monomer and also to give a solvent system that can maintain the morphology directing salts in the solution phase. The influence of the ratio of water to ethanol on the initial oxidation of the monomer and its subsequent electropolymerisation in a solution comprising 0.1 M $LiClO_4$ and 0.05 M PyEtCN is shown in Fig. 1(a) where cyclic voltammograms are presented. Increasing the ethanol content gives rise to lower initial oxidation potentials, with oxidation of the monomer beginning at approximately 0.86 V vs SCE with 70% ethanol, but increasing to about 1.02 V vs SCE when the ethanol content is reduced to 30%. The peak potentials show a similar trend, with a near linear increase in the peak oxidation potential with decreasing ethanol content. This is clearly evident in the inset in Fig. 1(a) where the peak oxidation potential is shown as a function of the ethanol content. The more facile oxidation of the monomer in the solution with 90% ethanol is consistent with the higher solubility of the monomer with increasing ethanol content. However, lower peak currents are seen with higher ethanol concentrations and this appears to be related to the difference in the dielectric constants of water at 80 and ethanol at 24. The coulombic repulsions between the radical cations generated on oxidation of the monomer are reduced in media with a high dielectric constant, such as water, and this facilitates radical-radical coupling [41] and therefore higher rates of electropolymerisation occur. Much lower rates of electropolymerisation are seen with the low dielectric constant solution of ethanol. It is also possible that the higher concentrations of ethanol may give rise to enhanced solubility of the oligomers, which in turn, would decrease the rate of electropolymerisation.

Although it was possible to form deposits of PPyEtCN with different ethanol contents, good solubility of both the monomer and inorganic salts was achieved only with about 30% ethanol content. The efficient rate of electropolymerisation with 30% ethanol is clearly evident in Fig. 1(b), where a near linear charge-time plot is seen. With increasing ethanol concentrations less efficient electropolymerisation is evident with deviations from the linear charge-time plots. However, on reducing the ethanol content to 20%, solubility issues became evident during electropolymerisation, as shown in Fig. 2, where a SEM micrograph is provided for PPyEtCN deposited from a solution containing 20% ethanol. While the bulk solution was homogenous with no visible evidence of globules, crystalline salt deposits were seen on the surface, with sizes varying from about 1 to 5 μm. These crystalline deposits were confirmed as inorganic salt deposits with a high chloride content, possibly containing $LiClO_4 \cdot 3H_2O$ or the less soluble NH_4ClO_4. During electropolymerisation the interfacial pH becomes more acidic and oligomers are formed and in this 20% ethanol solution where many of the reagents are close to their solubility limits, these changes appear to be sufficient to precipitate the salts onto the polymer. However, it was possible to prevent the formation of these hydrated salts by increasing the ethanol content to 30%.

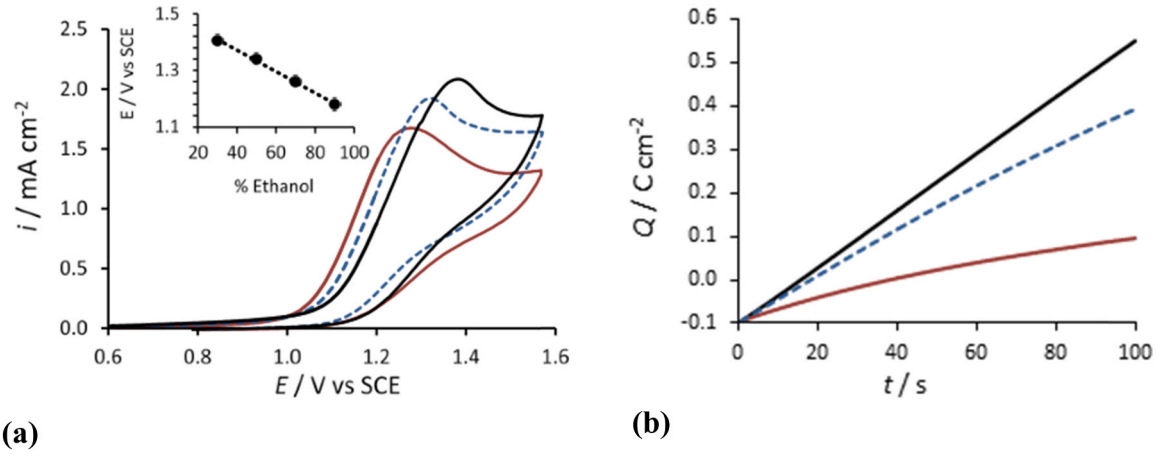

Fig. 1. Electropolymerisation of PyEtCN in 0.1 M $LiClO_4$ and 0.05 M PyEtCN (a) cyclic voltammograms recorded at 50 mV s^{-1} in 30% (black, solid), 50% (blue, dashed) and 70% ethanol (brown, solid), inset shows the peak potentials, *E*p, plotted as a function of the % ethanol, (b) charge-time plots recorded at 1.1 V vs SCE in 30% (black, solid), 50% (blue, dashed) and 100% ethanol (brown, solid).

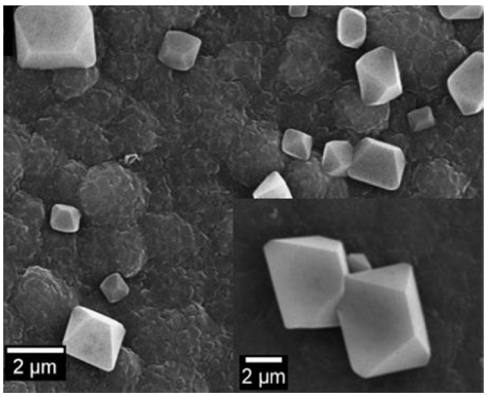

Fig. 2. SEM micrograph of salt structures dispersed on the surface of PPyEtCN formed at 0.85 V vs SCE in a water/ethanol (8:2) solution containing 0.02 M $LiClO_4$, 0.3 M $LiClO_4$, 0.3 M $NH_4H_2PO_4$ and 0.075 M PyEtCN.

3.2. Formation of nanowires and microwires

While the experimental conditions employed in Fig. 1 give rise to bulk PPyEtCN, it is possible to alter this morphology by using various electrolyte salts that have been employed in the formation of polypyrrole nanowires [42]. While these salts are normally used in aqueous solution, they are also suitably soluble in the ethanol-water solvent system, particularly when the sodium cations are replaced by ammonium ions. Typical current-time and charge-time curves recorded in 0.1 M PyEtCN and 0.07 M $LiClO_4$ with 0.2 M $NH_4H_2PO_4$, 0.2 M KH_2PO_4 or 0.39 M Cs_2CO_3 are shown in Fig. 3. Very good solubility was observed with $NH_4H_2PO_4$ and as illustrated, high rates of electropolymerisation were observed in this solution. Furthermore, no salt precipitates were formed during electropolymerisation. In the alkaline carbonate system, with a pH of 9.5, the measured currents are low and the corresponding charge-time plots clearly show that after the first 4 s, the charge consumed remains essentially constant, Fig. 3(b). This suggests that the deposited polymer becomes insulating. Clearly, the soluble ammonium salt with the slightly acidic pH gives rise to the more efficient formation of the PPyEtCN.

The PPyEtCN morphology was studied as a function of the initial monomer concentration, with different concentrations of $LiClO_4$ and $NH_4H_2PO_4$ and these data are summarised in Table 1. A selection of the corresponding SEM micrographs are presented in Fig. 4 where the influence of variations in the $LiClO_4$ concentration is highlighted. It is evident that a minimum concentration of $LiClO_4$ is necessary to produce the micro or nanowire morphology. At low concentrations of 0.015 M $LiClO_4$ the wires appear short and non-uniform in size, with a few much larger micro-sized wires, Fig. 4(a). As the concentration of perchlorate is increased to 0.02 M, the nanowires become more elongated and uniform. However, less uniform wires are seen with 0.1 M $LiClO_4$, Fig. 4(c).

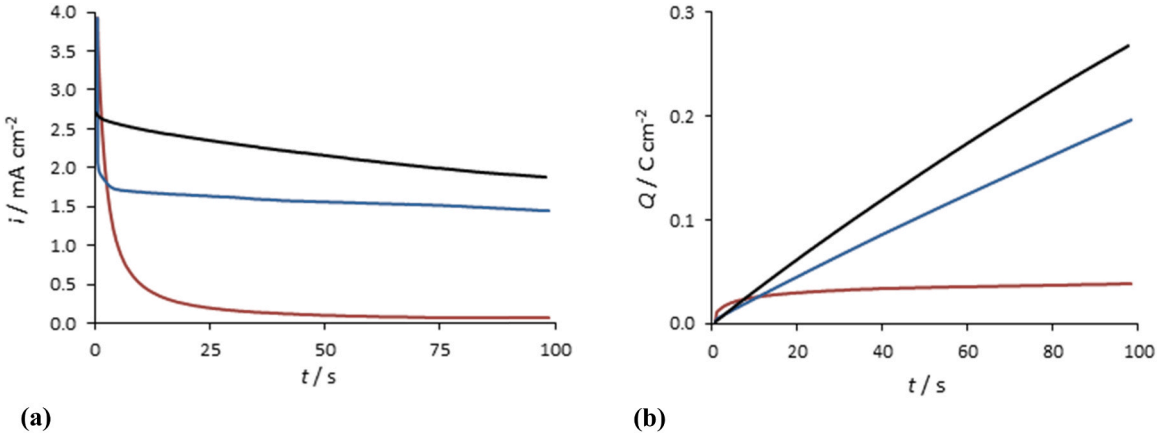

Fig. 3. (a) Current-time and (b) charge-time plots recorded at 0.85 V vs SCE in 0.1 M PyEtCN in water/ethanol (7:3) with 0.07 M $LiClO_4$ and 0.2 M $(NH_4)H_2PO_4$ (black) 0.2 M KH_2PO_4 (blue) and 0.39 M Cs_2CO_3 (brown).

Table 1
Summary of the morphology as a function of the electropolymerisation solutions for PPyEtCN deposited at 0.85 V vs SCE.

[PyEtCN]/ mM	[$LiClO_4$]/ mM	[$NH_4H_2PO_4$]/ mM	Ratio [$NH_4H_2PO_4$]/ [$LiClO_4$]	Morphology
75	20	90	4.5	Microwires/ mixed
75	20	200	10.0	Microwires/ mixed
75	20	250	12.5	Nanowires/ mixed
75	12	300	25.0	Nanowires/ non uniform
75	15	300	20.0	Nanowires/ non uniform
75	20	300	15.0	Nanowires/ uniform
75	40	500	12.5	Nanowires/ uniform
50	20	300	15.0	No polymer growth

A wire morphology with good uniform coverage is achieved using 0.075 M PyEtCN, 0.02 M $LiClO_4$ and 0.3 M $NH_4H_2PO_4$, as illustrated in Fig. 4(b).

The morphology of the polymer during the early stages of growth is evident in Fig. 4(d), where the electropolymerisation period was reduced to 1 min. In this case the nanowires can be clearly seen, having nucleated at nodules, and there is no evidence of any salt crystals. Indeed, the length of the wires is easily controlled by varying the electropolymerisation period, Table 2. In general, the wires become longer with greater diameters on extending the electropolymerisation period. Nanowires, with a diameter < 100 nm, are only evident with electropolymerisation periods up to approximately 4–5 min and on further growth, microwires, with diameters > 100 nm are obtained. Using EDX analysis, the elemental compositions of the nanowires and microwires were determined and these estimates are provided in Table 2. Five sites on each electrode surface were examined to give an average composition. Phosphorus and chlorine were detected indicating that both ClO_4^- and $H_2PO_4^-$ act as dopants. After a 5 min electropolymerisation period, the ratio of Cl:P is approximately 3:1, indicating a preference for the uptake and doping by ClO_4^-. This may be related to the speciation of the phosphate as the interfacial pH changes. As the pH decreases due to the electropolymerisation reaction, the concentration of the anionic form, $H_2PO_4^-$, will reduce to give increasing concentrations of the neutral H_3PO_4 molecule. During this early period, a thin bulk polymer is deposited and diffusion of the H^+ ions through the bulk polymer is relatively slow. As the nanowire morphology is adopted, removal of the H^+ becomes more efficient, the interfacial pH increases and the phosphate anions become available as dopants. As a result, the phosphate anions become the predominant dopants and this is seen in Table 2,

Table 2
The influence of the electropolymerisation period on the length, diameter and elemental composition of the PPyEtCN nanowires.

Time/min	Diameter/nm	Length/nm	Elemental composition/%		
			O	P	Cl
5	95 ± 8	400 ± 50	1.9	0.2	0.6
10	112 ± 8	580 ± 60			
20	122 ± 9	790 ± 70			
30	132 ± 8	1000 ± 90	6.2	2.0	0.6
50	148 ± 10	1550 ± 80			

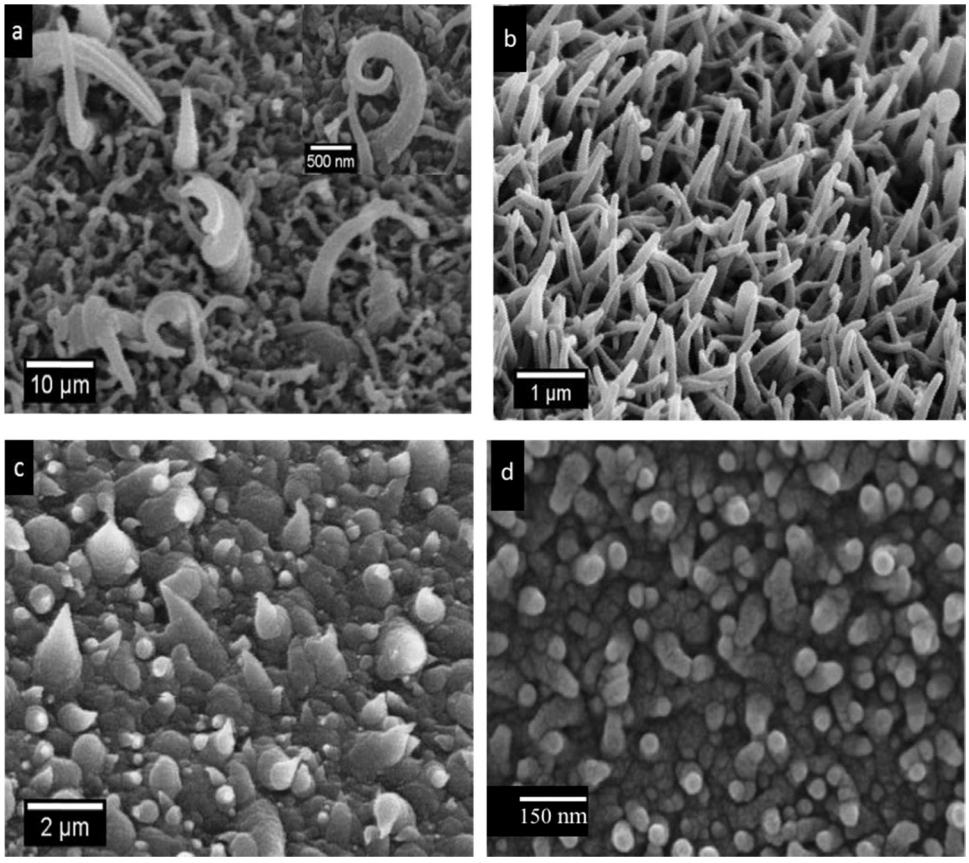

Fig. 4. SEM micrographs of PPyEtCN formed at 0.85 V vs SCE for 1 h in a water-ethanol mixture (7:3) with 0.075 M PyEtCN, 0.3 M $NH_4H_2PO_4$ and (a) 0.015 M $LiClO_4$, (b) 0.02 M $LiClO_4$, (c) 0.10 M $LiClO_4$ and (d) PPyEtCN formed for 1 min in 0.02 M $LiClO_4$, 0.3 M $NH_4H_2PO_4$ and 0.075 M PyEtCN.

where the ratio of phosphate is much higher after a 30 min electropolymerisation period. The high oxygen content is mainly associated with the phosphate and perchlorate dopants, but it may also indicate some overoxidation of the polymer. It is clearly evident from Tables 1, 2 and Fig. 4 that uniform nanowires and microwires can be obtained by employing $LiClO_4$ at relatively low concentrations of 0.02–0.04 M, to limit or confine the initial nucleation of the polymer nodules. Much higher phosphate levels are then needed to facilitate the growth of the emerging nanowires.

3.3. Characterisation of the nanowires and microwires

FTIR and RAMAN spectroscopy were used to characterise the PPyEtCN wires and these data are summarised in Table 3, while the corresponding spectra are presented in Fig. 5. The cyano group, C≡N, which has a characteristic IR absorption band, appears at 2246 cm^{-1} in the monomer and at 2251 cm^{-1} in the PPyEtCN nano/microwires, providing direct evidence that the cyano moiety has remained intact after electropolymerisation. The C═C stretching mode of the pyrrole ring is evident at 1610 cm^{-1} (monomer) and 1626 cm^{-1} (PPyEtCN), while the band at 1086 cm^{-1} is associated with the perchlorate anion. The absorption band at approximately 3100 cm^{-1} is related to the aromatic C—H vibrations [43]. A band was observed for the polymer at 1707 cm^{-1}, which is indicative of C═O and this can be related to the formation of carbonyl groups which in turn will disrupt the conjugation of the polymer chains [44]. RAMAN spectra were recorded for bulk polypyrrole and PPyEtCN and these data are also presented in Table 3. The band assignments for polypyrrole are in good agreement with that typically reported in the literature [45,46]. It is evident that the PPyEtCN nanowires/microwires retain the characteristic bands from 1600 to 1320 cm^{-1} associated with the pyrrole monomer unit, while the new band at 1149 cm^{-1} is probably associated with the ethyl chain from the cyano moiety [47] and the band at 1707 cm^{-1} is related to overoxidation of the polymer backbone structure. This is consistent with previous studies on the electropolymerisation of bulk N–substituted monomers, where overoxidation is commonly observed [47]. Indeed, it is well known that nitrile groups in polymeric materials can undergo hydrolysis reactions to produce carboxyl groups [48].

The electroactivity and redox properties of the PPyEtCN nanowires and microwires were studied using cyclic voltammetry and for comparison purposes similar experiments were carried out with PPy nanowires and bulk PPy. The PPyEtCN polymer films were deposited at 0.85 V vs SCE until charges of 0.05, 0.07 and 0.12 mC cm^{-2} were consumed, equivalent to electropolymerisation periods of 100 and 200 s (nanowires) and 300 s (microwires), respectively. These relatively low potentials were utilised to limit the overoxidation of the polymer. Inspection of the voltammograms of PPyEtCN, depicted in Fig. 6(a), reveals an oxidation wave centred at about 0.40 V vs SCE and a corresponding broad reduction wave, indicating a sluggish reduction of the nanowires/microwires. On increasing the charge to give higher amounts of polymer and longer microwires, there is a corresponding increase in the peak currents, but also the oxidation peak is shifted to higher potentials, indicating that it becomes progressively more difficult to oxidise and reduce the longer microwires. There is also a clear increase in the capacitance as higher amounts of the PPyEtCN are deposited. In Fig. 6(b), voltammograms are shown for the bulk PPy and PPy nanowires formed at 0.80 V vs SCE for 300 s. Clear oxidation and reduction peaks are observed in the vicinity of 0.20 V vs SCE for both the PPy nanowires and bulk PPy, with a slight shift in the peak potentials to more thermodynamically favourable values for the nanowire morphology. However, both films exhibit quasi-reversibility, with ΔEp values of 0.25 V and 0.30 V for the nanowire and bulk polymers, respectively. While both the PPy and PPyEtCN nanowires show redox activity, there is a considerable difference in the potentials at which these redox events are observed. For example, the reduction wave of the PPy nanowires occurs at about 0.25 V vs SCE, but it is centred at about 0.55 V vs SCE for the PPyEtCN nanowires/microwires.

Table 3
FTIR and RAMAN data recorded for PyEtCN, PPyEtCN and PPy.

Position/cm^{-1}			Assignments	
PyEtCN	PPyEtCN	PPy	FTIR	RAMAN
	1707	–		C═O stretch
	1576	1597		C═C stretch
	1499	1514		Skeletal band
	1379	1379		C—N stretch
	1295	1322		Ring stretching
	1149	–		C—H deformation
	–	1266		C—H in plane bending
	1075	1083		C—H in plane bending dication
	–	1054		C—H in plane bending cation
	974	984		Ring deformation cation
	–	940		Ring deformation dication
3100	–		C—H (α, β)	
2246	2251		C≡N	
–	1707		C═O	
1610	1626		C═C	
–	1086		ClO_4^-	
732	–		C—Hα	

3.4. Influence of toluene additions and formation of microtubes

As shown in our earlier paper [35], it is possible to alter the morphology of PPyEtCN by employing toluene as a template, where adsorption of toluene droplets at the electrode surface inhibits electropolymerisation and results in the formation of hollow microtubes around the droplets. On addition of toluene to the electropolymerisation solution and with vigorous stirring or sonication an emulsion is formed. In Fig. 7(a) current-time transients recorded in the toluene-containing solution, as an emulsion and a non-emulsion, are presented, where it is clearly evident that the emulsion alters the current response. The current is higher in the presence of the emulsion and this is probably related to the enhanced solubility of the monomer within the well dispersed droplets. However, as the dopants have limited solubility in toluene, the electropolymerisation proceeds only at the toluene and water/ethanol interface, enabling the formation of hollow tubes. As the hollow tubes and possibly some nanowires begin to nucleate, the current increases, giving an apparent peak after about 4 s. The corresponding SEM micrograph is shown in Fig. 7(b), where hollow tubes with diameters up to 3 μm are shown. Variations in the size of the microtubes is probably related to variations in the size of the toluene droplets. Indeed the mean size of the microtubes was easily controlled by varying the concentration of toluene, with average microtube diameters of 0.50, 1.86 and 3.88 μm for 60, 80 and 120 μL toluene in 10 mL, respectively. Interestingly, these hollow and vertically aligned microtubes were only formed in a stable toluene-containing emulsion with both the ClO_4^- dopant at low concentrations and the $H_2PO_4^-$ at higher levels. It was possible to deposit these microtubes at GC, Au, Pt and ITO electrodes, however, defects and scratch sites on the electrode surface gave rise to random microwires and nanowires, suggesting that the adsorbed toluene molecules direct initially the polymer growth, but the low $LiClO_4$ and higher $NH_4H_2PO_4$ concentrations are also required for the further growth of the tubes.

Using EDX the dopant profile was monitored as a function of the electropolymerisation period. For microtubes grown for 60, 120 and 300 s, the Cl content was estimated as 0.04%, 0.14% and 0.10%, respectively, while the P levels were approximated as 0.06%, 0.13% and 0.11%, respectively. This indicates that approximately equal amounts of ClO_4^- and $H_2PO_4^-$ are present as dopants during the first 300 s. This is somewhat different to that obtained with polypyrrole nanowires, where the ClO_4^- anions were the predominant dopants [23] and the PPyEtCN nano/microwires, Table 2. This appears to be connected with variations in the rates of electropolymerisation with the rate being lower for the

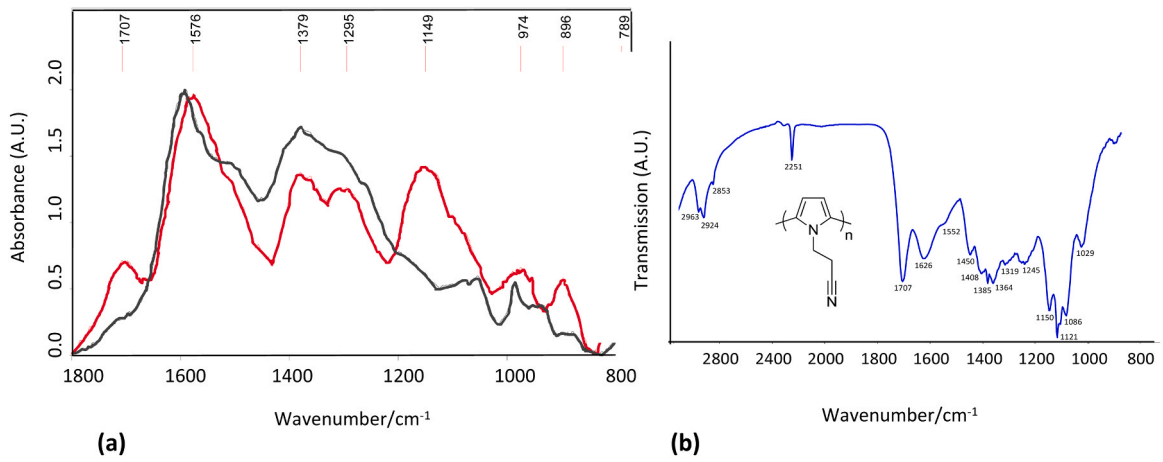

Fig. 5. (a) Raman spectra recorded for PPyEtCN (red trace) and PPy (black trace) recorded at 0.85 V vs SCE (b) FTIR spectrum recorded for PPyEtCN formed at 0.95 V vs SCE in 0.02 M $LiClO_4$, 0.3 M $NH_4H_2PO_4$ and 0.075 M PyEtCN in water/ethanol (7:3) solution.

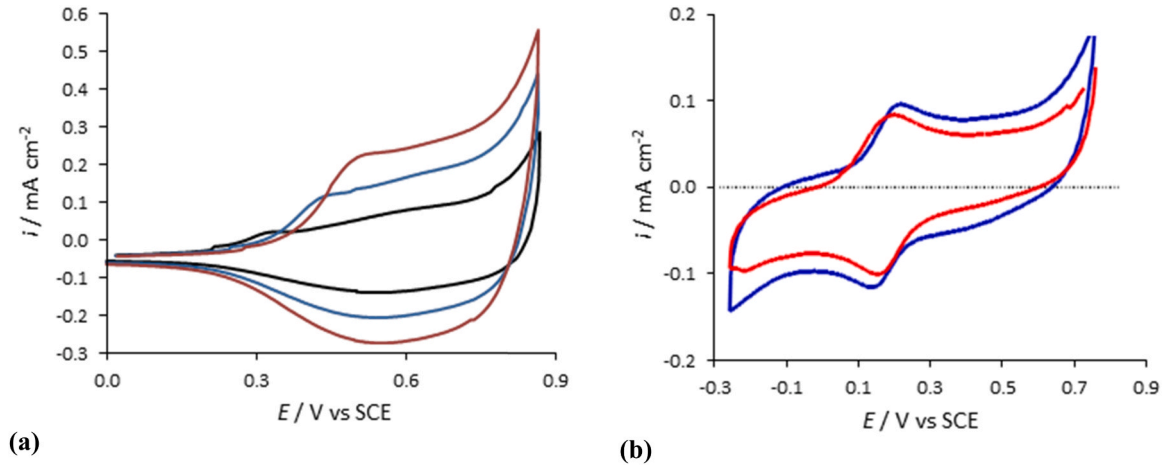

Fig. 6. Cyclic voltammograms recorded at 50 mV s^{-1} for (a) PPyEtCN deposited to charges of 0.05 (black trace), 0.07 (blue trace) and 0.12 mC cm^{-2} (brown trace) and (b) bulk (blue) and nanowire (red) polypyrrole films.

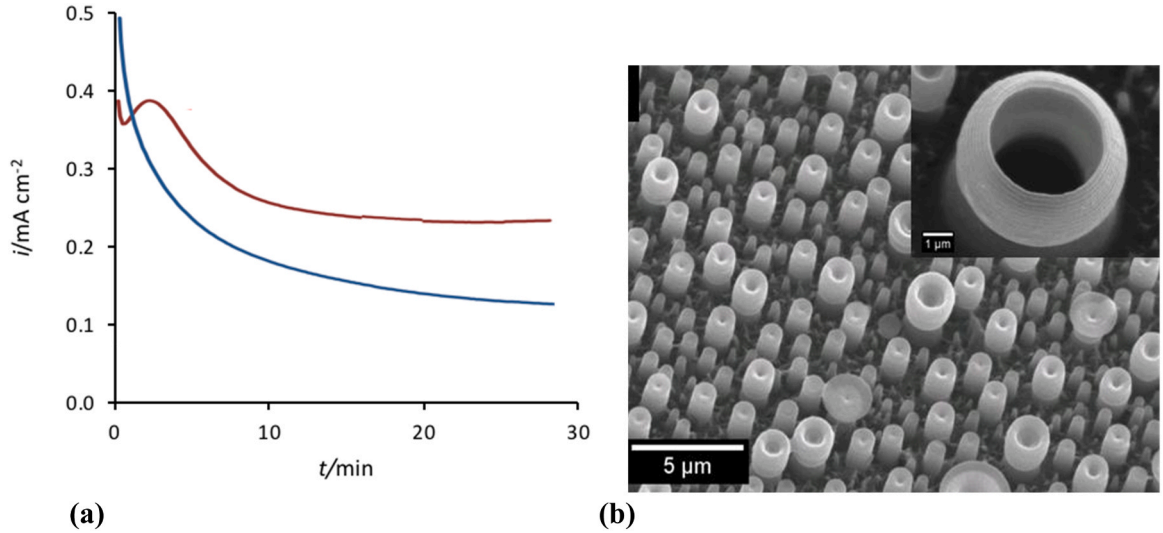

Fig. 7. (a) Current-time plots recorded at 0.85 V vs SCE in 0.075 M PyEtCN, 0.02 M $LiClO_4$ and 0.3 M $(NH_4)H_2PO_4$ and 80 µL toluene in 10 mL of electropolymerisation solution, with (brown) and without (blue) emulsion formation, (b) SEM micrograph of microtubes formed in the water-toluene emulsion.

PyEtCN microtubes. As detailed earlier, the initial decrease in the interfacial pH favours the ClO_4^- anion as the dopant. The higher levels of phosphate doping observed with the microtubes appears to be connected with a lower rate of interfacial acidification, enabling the uptake and doping by the $H_2PO_4^-$ anions. Indeed, this was confirmed by enhancing the rate of electropolymerisation and acidification using higher applied potentials. In this case, the ratio of Cl to P varied from 0.9 at 0.95 V, 4.2 at 1.1 V to 14.7 at 1.2 V vs SCE.

3.5. Electrodeposition of copper structures

Copper-modified polypyrrole films have been employed as biosensors [49] and in fuel cells [40], indicating that the addition of copper can be beneficial in a number of applications. Therefore, the PPyEtCN microwires and microtubes were used as substrates for the electrochemical reduction of copper ions and their ability to support the formation of copper deposits was compared with polypyrrole. The charge-time curves recorded during the electrodeposition of copper at − 0.135 V and − 0.20 V vs SCE are shown in Fig. 8 for the PPyEtCN microwires. While reduction of the Cu^{2+} ions occurs, the charges consumed are relatively small. At polarisation times approaching 150 s, the charge consumed is approximately 0.6 mC cm^{-2} at − 0.20 V, corresponding to about 3.1×10^{-9} mol cm^{-2} of deposited copper, neglecting the contribution of the oxygen and hydrogen reduction reactions. On comparing these data to bulk polypyrrole films (shown in the inset) it is evident that the polypyrrole substrates are more efficient, with near linear charge-time curves, indicating high rates of electrodeposition, with 0.62 C cm^{-2} of charge consumed after 150 s and a 1000-fold increase in the copper deposition rate compared to PPyEtCN.

Nevertheless, it is possible to deposit copper microstructures at PPyEtCN and in Fig. 9 the various structures deposited at bulk PPyEtCN and polypyrrole are shown. While the structures provided for polypyrrole were deposited at much lower overpotentials, at − 0.135 V and − 0.20 V vs SCE, the structures shown for the PPyEtCN were obtained at − 1.0 V and − 1.2 V vs SCE. As the reduction of Cu^{2+} in the presence of sulphates is generally accepted to proceed through two consecutive reactions, Eqs. (1) and (2), with Eq. (1) being the rate-determining step, with a standard reduction potential of − 0.087 V vs SCE, this highlights the significant overpotential required with the PPyEtCN system.

$$Cu^{2+} + e^- \rightarrow Cu^+ \; E^\circ = -0.087 \text{ V vs SCE} \quad (1)$$

$$Cu^+ + e^- \rightarrow Cu \; E^\circ = 0.281 \text{ V vs SCE} \quad (2)$$

For the polypyrrole system, Fig. 9(a), cube-like copper structures are clearly observed and these are well formed at − 0.135 V vs SCE within 10 s, while a branch-like morphology is observed at − 0.20 V vs SCE. On monitoring the evolution of this morphology, it was found that cube-like shapes are initially formed, followed by the formation of small clusters that begin to emerge to give stems, dispersed uniformly around the cubes. These stems continue to grow in size to give the main stem. At about 420 s, branching from the main stem occurs and the branched morphology continues to extend until the entire electrode is covered by the dendrites, as illustrated in Fig. 9(b). These leaf-like dendrites are normally formed at high overpotentials [50], typically 500 mV, indicating that polypyrrole is very efficient in the electrodeposition of copper ions.

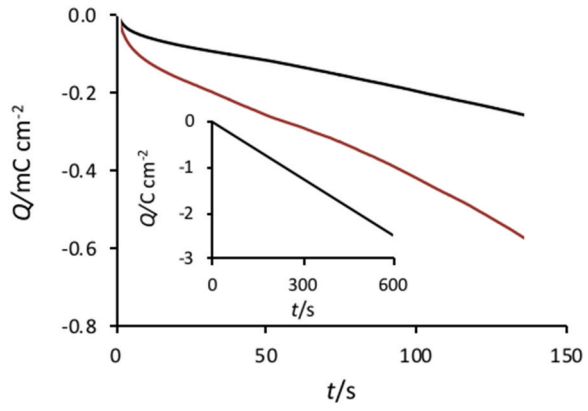

Fig. 8. Charge-time curves recorded for PPyEtCN at − 0.20 V (brown) and − 0.135 V (black) and inset shows the corresponding charge-time curves recorded for bulk polypyrrole at − 0.20 V vs SCE in 0.05 M $CuSO_4$ in 0.05 M Na_2SO_4, at a pH of 4.0.

As illustrated in Fig. 9(c), cube-like structures are also seen with the bulk PPyEtCN at short deposition times, but only at a much higher overpotential. These small cubes are well dispersed, but are relatively far apart, indicating few nucleation sites, despite the high overpotential. After deposition at − 1.0 V vs SCE for a 700 s period, the cubes appear to differ only slightly in size, suggesting an instantaneous nucleation mechanism, with a small number of initial nucleation sites. At a lower potential of − 1.2 V vs SCE, distorted leaf-like structures become evident, Fig. 9(f), but in addition other distorted structures are seen, as illustrated in Fig. 9(d) and (e). The branching structures seen in Fig. 9(b) were not seen with the more insulating PPyEtCN as sufficiently high rates of electrodeposition were not achieved to give diffusion limited aggregation.

It was also possible to generate copper structures at the PPyEtCN nanowires and microtubes and typical SEM micrographs are presented in Fig. 10(a) for the microwires and in Fig. 10(b)–(d) for the microtubes. In both cases large hierarchical flower-like structures are evident in this acidic solution. These structures appear to be wrapped around the outside of the microtubes. In most cases, only one large hierarchical structure is observed on each microtube, but when the microstructures are smaller and similar in size, two or more small structures can be supported on the microtube. This suggests competition between the growing structures. Once a single structure is nucleated it continues to propagate and grow, making it difficult for new nearby sites to nucleate. Surprisingly, the copper hierarchical structures can nucleate and grow at sites on the microtubes that are several microns from the electrode surface.

As illustrated in Fig. 11(a), these flower-like hierarchical structures are well distributed over the polymer surface, but with some variations in their size. It is also clear from the EDX spectrum, Fig. 11(b) that the deposit consists of copper oxides/hydroxides. This significant difference between the electrodeposition of copper at the bulk polypyrrole and PPyEtCN microtubes and microwires is not simply related to variations in the polymer morphologies. As illustrated in Fig. 11(c), a high density of copper deposits are readily formed at polypyrrole nanowires on cycling between the potential limits of − 0.40 and 0.10 V vs SCE, with well-formed triangular deposits formed after 10 cycles. On increasing the number of cycles, both the density and size of the copper structures increase with a loss in the clear triangle crystal habit. Evidently, the polypyrrole nanowires can support the formation of copper deposits and by altering the scan rate between 50 and 500 mV s^{-1} the copper structures can be altered from cubes, triangles, to sheets and sheet/spike-like structures, but flower-like hierarchical structures were not evident.

The formation of these flower-like hierarchical deposits has previously been linked to the parallel hydrogen evolution reaction [51]. The evolving hydrogen facilitates the stirring of the electrolyte to give a reduction in the thickness of the diffusion layer, while the hydrogen bubbles can cause voids in the forming copper structures. It appears that the more open microwire and microtube structures combined with the high overpotentials and the acidic bulk solution gives more efficient reduction of hydrogen ions and higher amounts of gaseous hydrogen molecules.

Although it is also possible to nucleate a variety of copper-based structures at both PPyEtCN microwires and microtubes, high overpotentials are required. This is associated with the conductivity of PPyEtCN, which is reported as 5.5×10^{-3} S cm^{-1}, significantly lower

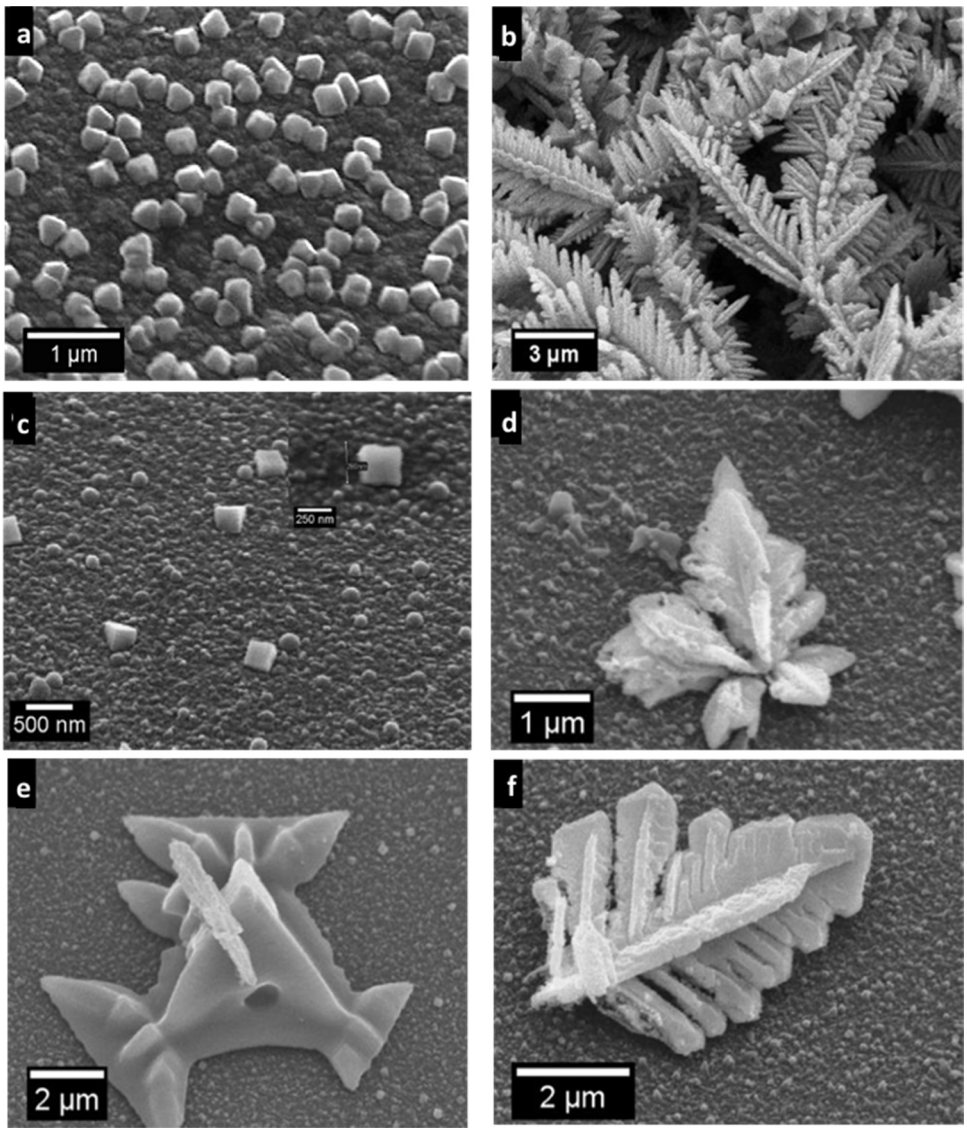

Fig. 9. SEM micrographs following electrodeposition of copper from 0.05 M Cu^{2+} in 0.05 M Na_2SO_4, pH 4.0 (a) at − 0.135 V for 10 s at PPy (b) at − 0.20 V for 360 s at PPy (c) at − 1.0 V for 700 s at PPyEtCN, (d)–(f) at − 1.2 V vs SCE for 700 s at PPyEtCN.

than that of the unsubstituted polymer [44]. It is also evident from the cyclic voltammograms presented in Fig. 6 that the PPyEtCN is reduced at relatively high potentials, compared to both the bulk and nanowire polypyrrole films, to give the insulating polymer and relatively low currents are observed at applied potentials lower than 0.20 V vs SCE. Therefore, it becomes increasingly more difficult to achieve the reduction of Cu^{2+} as lower potentials are applied, corresponding to more reduced and insulating PPyEtCN films. The number of nucleation sites typically increase as higher overpotentials are applied, however this is not seen with the reduced and insulating PPyEtCN.

Reduction of Cu^{2+} at the more insulating PPyEtCN may be facilitated by the phosphate dopants and/or the cyano groups. As the phosphate dopants are medium sized anions, some of these anions are likely to be maintained within the polymer matrix on reduction, giving mixed ion exchange. Indeed, Koehler et al. [52] observed the uptake of cations, which was accompanied by an increase in the surface roughness, on reduction of polypyrrole films doped with phosphates. Consequently, on reduction of PPyEtCN, Cu^{2+}, Na^+ or H^+ ions will be incorporated to achieve charge balance. Once a sufficient number of the Cu^{2+} ions are incorporated they may be reduced at polymer sites which are sufficiently porous to enable the reduction of Cu^{2+} and nucleation of the copper structures at the glassy carbon substrate. Moreover, it is well known that Cu(II) is readily reduced to Cu(I) by cyanide in aqueous solutions and that simple C-bonded cyano complexes of Cu(I) exist [53]. Therefore, the cyano group may also facilitate the reduction of copper ions to Cu_2O, as illustrated in Eqs. (3) and (4).

$$Cu^{2+} + e^- \rightarrow Cu^+ \quad (3)$$

$$2Cu^+ + H_2O \rightarrow Cu_2O + 2H^+ \quad (4)$$

The formation of the copper hierarchical structures at the top of the polymer microtubes are more difficult to explain. As conducting polymers are reduced, reduction starts at the electrode-polymer interface with the polymer adjacent to the electrode being reduced first to give a more insulating interface, making the overall reduction process more difficult. Indeed, this is evident in the cyclic voltammograms shown in Fig. 6, where a broad reduction wave is seen and this wave becomes broader with increasing electropolymerisation charge, indicating a slow conversion of the polymer from the oxidised to the reduced state. As the microtubes are at a considerable distance from this interface, complete reduction of the microtubes is unlikely to be achieved, giving a more conducting microtube, particularly towards the top of the microtube. The favourable complexation between the cyano group and copper ions

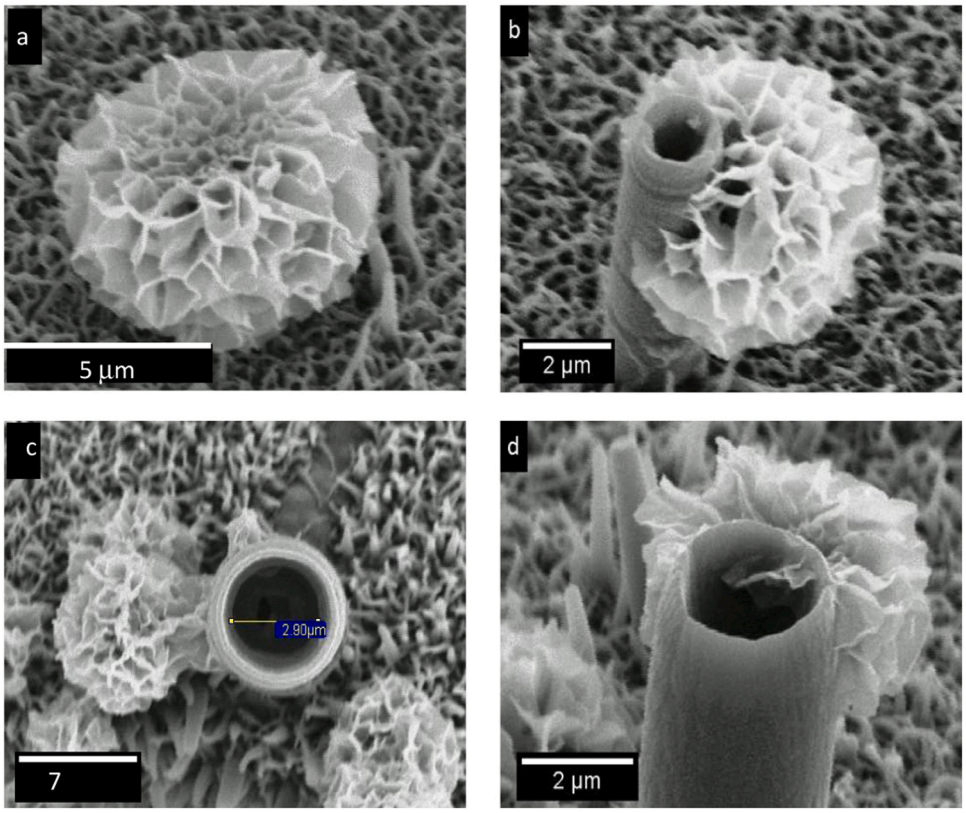

Fig. 10. SEM micrographs of electrodeposited copper on PPyEtCN nanowires (a) and on microtubes ((b)–(d)) from a solution of 0.05 M Cu^{2+} in 0.05 M H_2SO_4 at − 1.2 V vs SCE for 700 s.

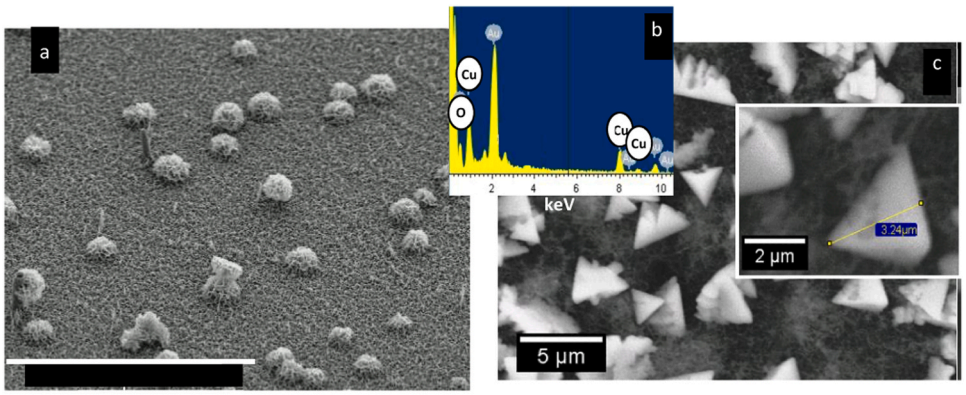

Fig. 11. SEM micrograph of copper electrodeposited from 0.05 M Cu^{2+} in 0.05 M H_2SO_4 (a) PPyEtCN nanowires at − 1.2 V vs SCE for 700 s (b) corresponding EDX spectrum (Au sputter deposited to enhance polymer conductivity) and (c) copper deposited at PPy by cycling in a potential window from 0.10 to − 0.40 V at 200 mV s^{-1} for 10 cycles.

and the formation of the cyano-Cu(I) appears to be sufficient to nucleate the copper structures close to the tip of the microtubes and nucleation of the initial Cu_2O deposits, Eqs. (3) and (4), which may then support further growth of the flower-like hierarchical structures. These events are consistent with this surprising growth of hierarchical copper structures at the top of the microtubes, at a considerable distance from the conducting substrate. Although the microtubes are hollow and have a base that has a thin polymer layer, there was no evidence from SEM or TEM analyses to indicate that the copper deposits nucleated at the base of the tubes, giving open tubes decorated with copper hierarchical structures, as illustrated in Fig. 10(c).

4. Conclusions

In this study it is shown that PPyEtCN can be formed in nanowire, microwire and microtube morphologies and further metallisation of the polymer can be achieved through copper electrodeposition. The nanowires and microwires are easily formed on electropolymerisation of the functionalised monomer by using relatively low concentrations of $LiClO_4$ and higher concentrations of $NH_4H_2PO_4$ in an ethanol-water solution. The final nanowires/microwires are doped by both the phosphate and perchlorate anions. On the addition of toluene to the electropolymerisation solution, which acts as a soft template, microtubes can be formed, with the diameter of the tubes being related to the size of the adsorbed toluene droplets. The electrodeposition of Cu^{2+} from a

slightly acidified sulphate solution, gives small copper-based cubes and larger leaf-like structures. On reducing the pH, hierarchical structures are formed on the microwires, while they also nucleate and deposit on the hollow microtubes, to give hierarchical copper decorated microtubes. While high overpotentials are employed, the wires and tubes can be decorated with different copper structures. Although the PPyEtCN polymer systems are less conducting than the corresponding polypyrrole films, the introduction of various copper nanostructures has the potential to enhance the electrocatalytic activity and properties of these hybrid materials. Their potential applications may extend from high performance supercapacitors to electrocatalysts in ethanol fuel cells. Moreover, supported copper structures are finding applications in the electrochemical reduction of CO_2 and the water oxidation reaction.

Author statement

All authors have contributed to this work. Conception and design of study (CBB, BAE), acquisition of data (CPM, KMH), Analysis and interpretation of data (CBB, DR, BAE, CPM), drafting manuscript (CBB, CPM, KMH, DR), revising manuscript (CBB, CPM).

Declaration of Competing Interest

The authors declare that they have no known competing financial interests or personal relationships that could have appeared to influence the work reported in this paper.

Acknowledgements

The authors wish to acknowledge the financial support provided by the Environmental Protection Agency, Ireland (2007-DRP-1-S5), Science Foundation Ireland-funded National Access Programme (NAP 353 at Tyndall National Institute, Ireland) and the Irish Research Council (RS/2012/79).

References

[1] A. Afzal, F.A. Abuilaiwi, A. Habib, M. Awais, S.B. Waje, M.A. Atieh, Polypyrrole/carbon nanotube supercapacitors: technological advances and challenges, J. Power Sources 352 (2017) 174–186, https://doi.org/10.1016/j.jpowsour.2017.03.128.
[2] H. Park, J.W. Kim, S.Y. Hong, G. Lee, D.S. Kim, J.H. Oh, S.W. Jin, Y.R. Jeong, S. Y. Oh, J.Y. Yun, J.S. Ha, Microporous polypyrrole-coated graphene foam for high-performance multifunctional sensors and flexiblesupercapacitors, Adv. Funct. Mater. 28 (2018), 1707013, https://doi.org/10.1002/adfm.201707013.
[3] B.K. Shrestha, R. Ahmad, S. Shrestha, C.H. Park, C.S. Kim, In situ synthesis of cylindrical spongy polypyrrole doped protonated graphitic carbon nitride for cholesterol sensing application, Biosens. Bioelectron. 94 (2017) 686–693, https://doi.org/10.1016/j.bios.2017.03.072.
[4] E. Andreoli, D.A. Rooney, W. Redington, R. Gunning, C.B. Breslin, Electrochemical deposition of hierarchical micro/nanostructures of copper hydroxysulfates on polypyrrole–polystyrene sulfonate films, J. Phys. Chem. C 115 (2011) 8725–8734, https://doi.org/10.1021/jp200465n.
[5] E. Andreoli, V. Annibaldi, D.A. Rooney, C.B. Breslin, Electrochemical fabrication of copper-based hybrid microstructures and mechanism of formation of related hierarchical structures on polypyrrole films, J. Phys. Chem. C 115 (2011) 20076–20083, https://doi.org/10.1021/jp204092x.
[6] V. Ratautaite, G. Bagdziunas, A. Ramanavicius, A. Ramanaviciene, An application of conducting polymer polypyrrole for the design of electrochromic pH and CO_2 sensors, J. Electrochem. Soc. 166 (2019) B297–B303, https://doi.org/10.1149/2.1221904jes.
[7] G. Eom, C. Oh, J. Moon, H. Kim, M.K. Kim, K. Kim, J.-W. Seo, T. Kang, H.J. Lee, Highly sensitive and selective detection of dopamine using overoxidized polypyrrole/sodium dodecyl sulfate-modified carbon nanotube electrodes, J. Electroanal. Chem. 848 (2019), 113295, https://doi.org/10.1016/j.jelechem.2019.113295.
[8] C.C. Harley, V. Annibaldi, T. Yu, C.B. Breslin, The selective electrochemical sensing of dopamine at a polypyrrole film doped with an anionic β–cyclodextrin, J. Electroanal. Chem. 855 (2019), 113614, https://doi.org/10.1016/j.jelechem.2019.113614.
[9] G.M. Hendy, C.B. Breslin, The incorporation and controlled release of dopamine from a sulfonated β–cyclodextrin–doped conducting polymer, J. Polym. Res. 26 (2019) 61, https://doi.org/10.1007/s10965-019-1733-5.
[10] E.M. Ryan, C.B. Breslin, The incorporation of drug molecules with poor water solubility into polypyrrole as dopants: indomethacin and sulindac, Electrochim. Acta 296 (2019) 848–855, https://doi.org/10.1016/j.electacta.2018.11.107.
[11] U. Carragher, C.B. Breslin, Polypyrrole doped with dodecylbenzene sulfonate as a protective coating for copper, Electrochim. Acta 291 (2018) 362–372, https://doi.org/10.1016/j.electacta.2018.08.155.
[12] X. Yang, X. Liu, T. Qin, X. Zhang, W. Zhang, W. Zheng, Polypyrrole coated hollow S/Co-doped carbon nanocages excels for packaging high-performance lithium sulfur batteries, Nanotechnology 31 (2020), 275404, https://doi.org/10.1088/1361-6528/ab849f.
[13] R.B. Choudhary, S. Ansari, B. Purty, Robust electrochemical performance of polypyrrole (PPy) and polyindole (PIn) based hybrid electrode materials for supercapacitor application: a review, J. Energy Storage 29 (2020), 101302, https://doi.org/10.1016/j.est.2020.101302.
[14] H. Bagheri, Z. Ayazi, M. Naderi, Conductive polymer-based microextraction methods: a review, Anal. Chim. Acta 767 (2013) 1–13, https://doi.org/10.1016/j.aca.2012.12.013.
[15] Z.-H. Huang, Y. Song, X.-X. Xu, X.-X. Liu, Ordered polypyrrole nanowire arrays grown on a carbon cloth substrate for a high-performance pseudocapacitor electrode, ACS Appl. Mater. Interfaces 7 (2015) 25506–25513, https://doi.org/10.1021/acsami.5b08830.
[16] J. Huang, K. Wang, Z. Wei, Conducting polymer nanowire arrays with enhanced electrochemical performance, J. Mater. Chem. 20 (2010) 1117–1121, https://doi.org/10.1039/b919928d.
[17] Q. Xu, G. Meng, F. Han, X. Zhao, M. Kong, X. Zhu, Controlled fabrication of gold and polypyrrole nanowires with straight and branched morphologies via porous alumina template-assisted approach, Mater. Lett. 63 (2009) 1431–1434, https://doi.org/10.1016/j.matlet.2009.03.026.
[18] W. Ahmed El-Said, C.-H. Yea, M. Jung, H. Kim, J.-W. Choi, Analysis of effect of nanoporous alumina substrate coated with polypyrrole nanowire on cell morphology based on AFM topography, Ultramicroscopy 110 (2010) 676–681, https://doi.org/10.1016/j.ultramic.2010.02.031.
[19] M. Trueba, A.L. Montero, J. Rieumont, Pyrrole nanoscaled electropolymerization: effect of the proton, Electrochim. Acta 49 (2004) 4341–4349, https://doi.org/10.1016/j.electacta.2004.03.043.
[20] Z. Niu, J. Liu, L.A. Lee, M.A. Bruckman, D. Zhao, G. Koley, Q. Wang, Biological templated synthesis of water-soluble conductive polymeric nanowires, Nano Lett. 7 (2007) 3729–3733, https://doi.org/10.1021/nl072134h.
[21] J.P. Jyothibasu, R.-H. Lee, Green synthesis of polypyrrole tubes using curcumin template for excellent electrochemical performance in supercapacitors, J. Mater. Chem. A 8 (2020) 3186–3202, https://doi.org/10.1039/c9ta11934e.
[22] A.D.W. Carswell, E.A. O'Rear, B.P. Grady, Adsorbed surfactants as templates for the synthesis of morphologically controlled polyaniline and polypyrrole nanostructures on flat surfaces: from spheres to wires to flat films, J. Am. Chem. Soc. 125 (2003) 14793–14800, https://doi.org/10.1021/ja0365983.
[23] C. Debiemme-Chouvy, Template-free one-step electrochemical formation of polypyrrole nanowire array, Electrochem. Commun. 11 (2009) 298–301, https://doi.org/10.1016/j.elecom.2008.11.030.
[24] L. Al-Mashat, C. Debiemme-Chouvy, S. Borensztajn, W. Wlodarski, Electropolymerized polypyrrole nanowires for hydrogen gas sensing, J. Phys. Chem. C 116 (2012) 13388–13394, https://doi.org/10.1021/jp3015854.
[25] D.-H. Nam, M.-J. Kim, S.-J. Lim, I.-S. Song, H.-S. Kwon, Single-step synthesis of polypyrrole nanowires by cathodic electropolymerization, J. Mater. Chem. A 1 (2013) 8061–8068, https://doi.org/10.1039/c3ta11227f.
[26] Y. Li, Y. Wang, C. Bian, J. Stejskal, Y. Zheng, X. Jing, Azo dye aggregates and their roles in the morphology and conductivity of polypyrrole, Dyes Pigments 177 (2020), 108329, https://doi.org/10.1016/j.dyepig.2020.108329.
[27] J. Kopecká, D. Kopecký, M. Vrňata, P. Fitl, J. Stejskal, M. Trchová, P. Bober, Z. Morávková, J. Prokeš, I. Sapurina, Polypyrrole nanotubes: mechanism of formation, RSC Adv. 4 (2014) 1551–1558, https://doi.org/10.1039/c3ra45841e.
[28] Y. Li, P. Bober, M. Trchová, J. Stejskal, Polypyrrole prepared in the presence of methyl orange and ethyl orange: nanotubes versus globules in conductivity enhancement, J. Mater. Chem. C 5 (2017) 4236–4245, https://doi.org/10.1039/c7tc00206h.
[29] J.F.F. Ribeiro, J.R.S. Melo, K.B.O. Silva, P.E.C. Filho, B.S. Santos, G.A.L. Pereira, R. T. Ribeiro, L.C. Silva, A. Fontes, CdTe quantum dots in a glassy carbon electrochemical platform modified by N-substituted polypyrrole: increasing the functional active surface for conjugation, Surf. Interfaces 19 (2020), 100532, https://doi.org/10.1016/j.surfin.2020.100532.
[30] F. Lallemand, D. Auguste, C. Amato, L. Hevesi, J. Delhalle, Z. Mekhalif, Electrochemical synthesis and characterization of N-substituted polypyrrole derivatives on nickel, Electrochim. Acta 52 (2007) 4334–4341, https://doi.org/10.1016/j.electacta.2006.12.010.
[31] G.Y. Han, G.Q. Shi, L.T. Qu, J.Y. Yuan, F.E. Chen, P.Y. Wu, Electrochemical polymerization of chiral pyrrole derivatives in electrolytes containing chiral camphor sulfonic acid, Polym. Int. 53 (2004) 1554–1560, https://doi.org/10.1002/pi.1597.
[32] G. Zotti, S. Zecchin, G. Schiavon, B. Vercelli, A. Berlin, E. Dalcanale, L. Groenendaal, Potential-driven conductivity of polypyrroles, poly-N-alkylpyrroles, and polythiophenes: role of the pyrrole NH moiety in the doping-charge dependence of conductivity, Chem. Mater. 15 (2003) 4642–4650, https://doi.org/10.1021/cm030336i.
[33] J. Husson, S. Lakard, S. Monney, C.C. Buron, B. Lakard, Elaboration and characterization of carboxylic acid-functionalized polypyrrole films, Synth. Met. 220 (2016) 247–254, https://doi.org/10.1016/j.synthmet.2016.06.017.
[34] D.A. Walker, C. D'Silva, Electrochemical and physical properties of N-substituted arylmethylene pyrrole polymers and N-alkylmethine pyrrole copolymers, Electrochim. Acta 116 (2014) 175–182, https://doi.org/10.1016/j.electacta.2013.11.013.

[35] C.P. McCarthy, N.B. McGuinness, P.B. Carolan, C.M. Fox, B.E. Alcock-Earley, C. B. Breslin, A.D. Rooney, Electrochemical deposition of hollow N-substituted polypyrrole microtubes from an acoustically formed emulsion, Macromolecules 46 (2013), https://doi.org/10.1021/ma302493e.
[36] O. Ouerghi, A. Senillou, N. Jaffrezic-Renault, C. Martelet, H. Ben Ouada, S. Cosnier, Gold electrode functionalized by electropolymerization of a cyano N-substituted pyrrole: application to an impedimetric immunosensor, J. Electroanal. Chem. 501 (2001) 62–69, https://doi.org/10.1016/S0022-0728(00)00485-X.
[37] D. Melling, S.A. Wilson, E.W.H. Jager, Controlling the electro-mechanical performance of polypyrrole through 3- and 3,4-methyl substituted copolymers, RSC Adv. 5 (2015) 84153–84163, https://doi.org/10.1039/c5ra15587h.
[38] C.P. McCarthy, N.B. McGuinness, B.E. Alcock-Earley, C.B. Breslin, A.D. Rooney, Facile template-free electrochemical preparation of poly[N-(2-cyanoethyl) pyrrole] nanowires, Electrochem. Commun. 20 (2012) 79–82, https://doi.org/10.1016/j.elecom.2012.03.047.
[39] X. Li, L. Feng, K. Wang, W. Wang, One-step synthesis of hollow N-substituted polypyrrole@β-FeOOH microspheres, Synth. Met. 259 (2020), 116226, https://doi.org/10.1016/j.synthmet.2019.116226.
[40] A. El Attar, L. Oularbi, S. Chemchoub, M. El Rhazi, Preparation and characterization of copper oxide particles/polypyrrole (Cu_2O/PPy) via electrochemical method: application in direct ethanol fuel cell, Int. J. Hydrog. Energy 45 (2020) 8887–8898, https://doi.org/10.1016/j.ijhydene.2020.01.008.
[41] F. Beck, M. Oberst, R. Jansen, On the mechanism of the filmforming electropolymerization of pyrrole in acetonitrile with water, Electrochim. Acta 35 (1990) 1841–1848, https://doi.org/10.1016/0013-4686(90)87088-J.
[42] C. Debiemme-Chouvy, A. Fakhry, F. Pillier, Electrosynthesis of polypyrrole nano/micro structures using an electrogenerated oriented polypyrrole nanowire array as framework, Electrochim. Acta 268 (2018) 66–72, https://doi.org/10.1016/j.electacta.2018.02.092.
[43] G. Fabregat, C. Alemán, M.T. Casas, E. Armelin, Controlling the morphology of poly(N-cyanoethylpyrrole), J. Phys. Chem. B 116 (2012) 5064–5070, https://doi.org/10.1021/jp3008688.
[44] D. Aradilla, F. Estrany, E. Armelin, R. Oliver, J.I. Iribarren, C. Alemán, Characterization and properties of poly[N-(2-cyanoethyl)pyrrole], Macromol. Chem. Phys. 211 (2010) 1663–1672, https://doi.org/10.1002/macp.201000015.
[45] L. Dauginet-De Pra, S. Demoustier-Champagne, Investigation of the electronic structure and spectroelectrochemical properties of conductive polymer nanotube arrays, Polymer 46 (2005) 1583–1594, https://doi.org/10.1016/j.polymer.2004.12.016.
[46] S. Demoustier-Champagne, P.-Y. Stavaux, Effect of electrolyte concentration and nature on the morphology and the electrical properties of electropolymerized polypyrrole nanotubules, Chem. Mater. 11 (1999) 829–834, https://doi.org/10.1021/cm9807541.
[47] B. Teixeira-Dias, C. Alemán, F. Estrany, D.S. Azambuja, E. Armelin, Microstructures of poly(N-methylpyrrole) and their interaction with morphine, Electrochim. Acta 56 (2011) 5836–5843, https://doi.org/10.1016/j.electacta.2011.04.069.
[48] P.R. Sruthi, S. Anas, An overview of synthetic modification of nitrile group in polymers and applications, J. Polym. Sci. 58 (2020) 1039–1061, https://doi.org/10.1002/pol.20190190.
[49] F. Meng, W. Shi, Y. Sun, X. Zhu, G. Wu, C. Ruan, X. Liu, D. Ge, Nonenzymatic biosensor based on Cu_xO nanoparticles deposited on polypyrrole nanowires for improving detection range, Biosens. Bioelectron. 42 (2013) 141–147, https://doi.org/10.1016/j.bios.2012.10.051.
[50] N.D. Nikolić, K.I. Popov, L.J. Pavlović, M.G. Pavlović, Morphologies of copper deposits obtained by the electrodeposition at high overpotentials, Surf. Coat. Technol. 201 (2006) 560–566, https://doi.org/10.1016/j.surfcoat.2005.12.004.
[51] N.D. Nikolić, V.M. Maksimović, L. Avramović, Correlation of morphology and crystal structure of metal powders produced by electrolysis processes, Metals 11 (2021), https://doi.org/10.3390/met11060859.
[52] S. Koehler, M. Ueda, I. Efimov, A. Bund, An EQCM study of the deposition and doping/dedoping behavior of polypyrrole from phosphoric acid solutions, Electrochim. Acta 52 (2007) 3040–3046, https://doi.org/10.1016/j.electacta.2006.09.044.
[53] S.F. Huang, H.H. Wei, W. Yu, A new cyano-bridged one-dimensional polymeric mixed-valence CuII/CuI complex formed from reduction of a binuclear CuII complex with sodium cyanide, Polyhedron 16 (1997) 1747–1753, https://doi.org/10.1016/S0277-5387(96)00455-X.